JOC The Journal of Organic Chemistry
Cite This: J. Org. Chem. 2019, 84, 687−697
Article
pubs.acs.org/joc

Indolizine-Cyanine Dyes: Near Infrared Emissive Cyanine Dyes with Increased Stokes Shifts

Jacqueline Gayton,[†,∥] Shane A. Autry,[†,∥] William Meador,[†] Sean R. Parkin,[‡] Glake Alton Hill, Jr.,[§] Nathan I. Hammer,[†] and Jared H. Delcamp*[,†]

[†]Department of Chemistry and Biochemistry, University of Mississippi, University, Mississippi 38677, United States
[‡]Department of Chemistry, University of Kentucky, Lexington, Kentucky 40506, United States
[§]Department of Chemistry, Jackson State University, Jackson, Mississippi 39217, United States

Supporting Information

ABSTRACT: Molecular engineering strategies designed to red-shift cyanine dye absorptions and emissions further into the near-infrared (NIR) spectral region are explored. Through the use of a novel donor group, indolizine, with varying cyanine bridge lengths, dye absorptions and emissions, were shifted deeper into the NIR region than common indoline-cyanines. Stokes shifts resulting from intramolecular steric interactions of up to ∼60 nm in many cases were observed and explained computationally. Molecular brightnesses of up to 5800 deep into the NIR region were observed. Structure−property relationships are explored for the six indolizine-cyanine dyes with varying cyanine bridge length and indolizine substituents showing broad absorption and emission tunability. The dyes are characterized by crystallography, and the photophysical properties are probed by varying solvent for absorption and emission studies. Computational data show involvement of the entire indolizine π-system during light absorption, which suggests these systems can be tunable even further into the NIR region through select derivatizations.

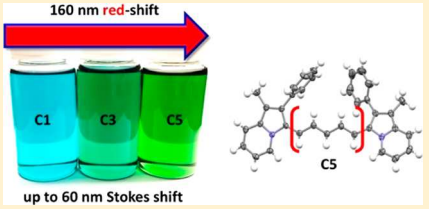

INTRODUCTION

Near infrared (NIR) emissive materials are a widely researched class of compounds with applications in an array of areas[1] including biological imaging, communications, and secure displays.[2−7] Dye designs based on cyanine structures are ubiquitous because of the intense molar absorptivity of these structures in the NIR region.[1] Additionally, the cyanine dye absorption wavelength is highly tunable based on methine chain length selection.[8] The tunability, rapid synthesis, facile bioconjugation, intense molar absorptivities (ε), strong NIR emissions, and high molecular brightness (MB) values make this class of dyes attractive for further exploration as NIR emissive materials.[8,9] In addition to deeper NIR absorption and emission, dyes with large Stokes shifts and high quantum yields are in high demand.[9−12] For many applications, longer wavelength absorptions allow for access to differential dye properties relative to currently available dyes, and a larger Stokes shift provides dramatically higher resolution images in biological applications by reducing background signals.[5,13,14] Importantly, a significant MB is needed to give high resolution images with smaller amounts of emissive material.[15] A balance between long wavelength use, Stokes shifts, and quantum yield must be struck for many functional materials in the NIR region, since the energy gap rule dictates diminished quantum yields as wavelengths increase.[16−19] Stokes shifts, which arise from molecular reorganizations, also tend to diminish quantum yields as the Stokes shift increases in magnitude. Introduction of molecular design elements which can increase Stokes shifts and the wavelength of both absorption and emission, while retaining a reasonable molecular brightness, can address a fundamental need in NIR emissive dye design.[20] Both the Stokes shift and lower energy absorption/emission challenges can be addressed by replacing the indoline donor of typical indoline cyanine dyes (such as FDA approved, commercially available, and widely used indocyanine green **ICG**) with a fully conjugated indolizine donor to delocalize the frontier molecular orbitals further (Figure 1). **ICG** serves as a good benchmarking cyanine dye since it is one of the most widely used cyanines over the past six decades with multiple reviews concerning the utility of this compound.[21,22] In the specific case of our study, the single nitrogen heteroatom donor groups of indoline-cyanines can be directly compared to the single nitrogen heteroatom donor groups of novel indolizine-cyanine dyes since the donor heteroatom remains constant and a similar number of π-bonds are present in both donor groups. Additionally, the polycyclic indolizine donor provides a steric presence near the cyanine bridge, which requires either a deviation from planarity of the π-system or nonideal bond angles. Strain such as this in the ground state often affects excited state geometries differently, leading to increased reorganizations upon photoexcitation and thus enhanced Stokes shifts.[23,24]

Recently, our group published a series of squaraine dyes using an indolizine heterocycle as a donor in place of an indoline donor.[25] The indolizine donor allows for red shifts

Received: September 30, 2018
Published: December 12, 2018

DOI: 10.1021/acs.joc.8b02521
J. Org. Chem. 2019, 84, 687−697

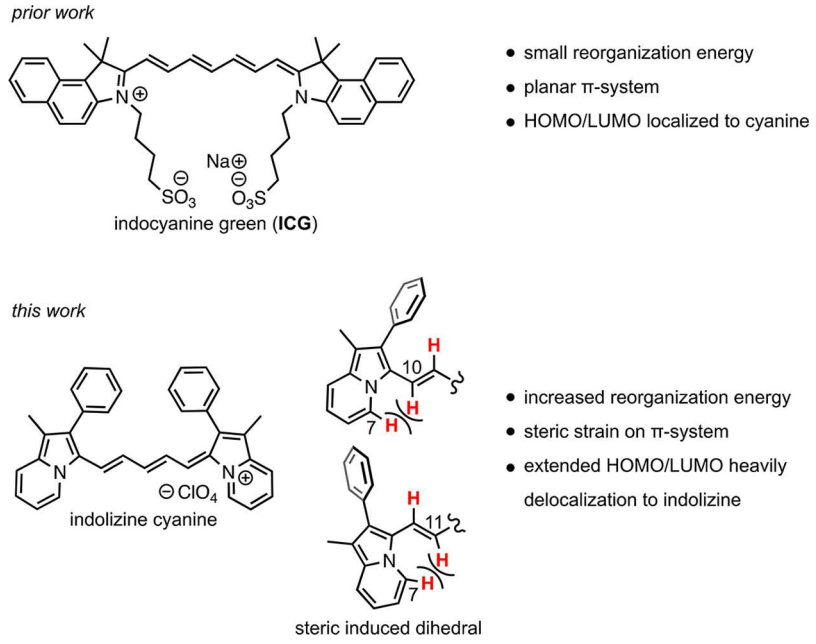

Figure 1. Comparison of an indoline cyanine dye and an indolizine cyanine dye. Hydrogens are drawn in for a portion of the indolizine cyanine on the right to show steric interactions. The indolizines are drawn in a *cis* conformation with a C7−C10 closest interaction as observed by crystallography for this specific compound. A second conformation exists for a C7−C11 close interaction which is also observed via crystallography in an example (see below).

farther into the NIR region due to the proaromatic nature of the indolizine, which generates an aromatic stabilized pyridinium ring after electron donation.[26] Additionally, an increased Stokes shift was observed, due in part to the planarization of aryl substituents on the indolizine ring in the excited state. This is significant, as indoline-squaraine dyes are known for very narrow energy gaps between the absorption and emission spectrum. Importantly, the molar absorptivities and quantum yields (and by default the MB, where MB = $\varepsilon \times \Phi$) remained high despite these changes. We reasoned that a similar strategy could be employed with cyanine bridges in place of the squaraine bridge. The cyanine-bridged dyes are attractive targets due to the simplistic tunability of the absorption wavelength by methine-bridge length selection. This type of straightforward absorption spectrum tuning is attractive, but is challenging to achieve with squaraine bridges. In this work, a series of dyes utilizing a constant indolizine donor structure with cyanine bridges between the donors of varying lengths with one, three, and five carbons (**C1**, **C3**, and **C5**) were prepared to probe the effects of methine bridge length on optical properties (Figure 2). Additionally, the electronic activity of positions on the indolizine donors are evaluated ranging from electron donating to electron withdrawing (**PhOMeIndz-C5**, **PhCNIndz-C5**, and **PhIndzOMe-C5**) in order to probe structure−property relationships on the dye optical properties.

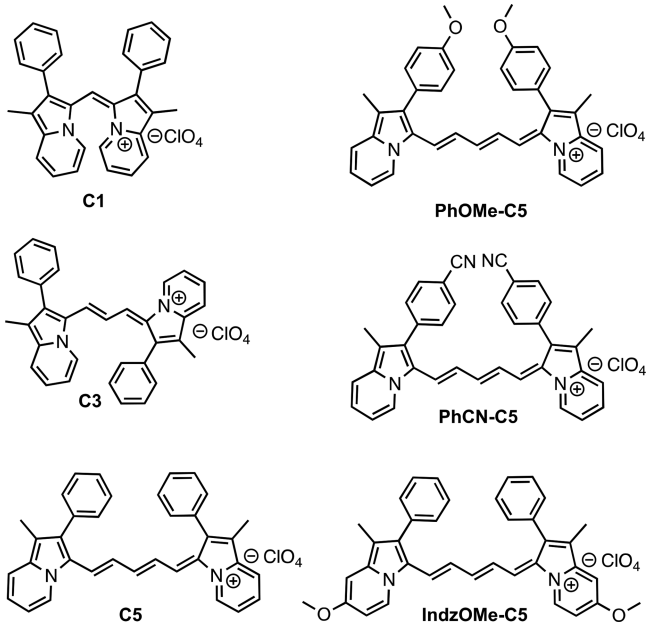

Figure 2. Target indolizine cyanine dyes.

RESULTS AND DISCUSSION

Target dyes **C1**, **C3**, and **C5** were synthesized from a known phenyl indolizine (**PhIndz**), which is available in two steps from commercially available 2-ethylpyridine (**1** when R′ = H) and 2-bromoacetophenone (**2** when R = H) via an *N*-alkylation reaction followed by a base catalyzed condensation reaction sequence (Figure 3).[23] **PhIndz** was then reacted with methine bridge precursors **4**, **5**, and **6** in the presence of perchloric acid to give **C1**, **C3**, and **C5**, respectively, in moderate to high yield (38−85%). **PhOMe-C5** and **PhCN-C5** follow the same synthetic route as **C5** beginning with known indolizine building blocks **PhOMeIndz** (**3** when R = OMe and R′ = H) and **PhCNIndz** (**3** when R = CN and R′ = H), respectively. The synthesis of **IndzOMe-C5** began with the alkylation of commercially available 2-ethyl-4-methoxypyridine (**1** when R′ = OMe) with 2-bromoacetophenone, followed by cyclization to give **PhIndzOMe**. Reaction of **PhIndzOMe** with iminium salt **6** afforded **IndzOMe-C5** in low isolated yield, presumably due to the low stability of the indolizine precursor in the reaction mixture, as the starting indolizine was consumed during the reaction. In general, the starting

DOI: 10.1021/acs.joc.8b02521
J. Org. Chem. 2019, 84, 687−697

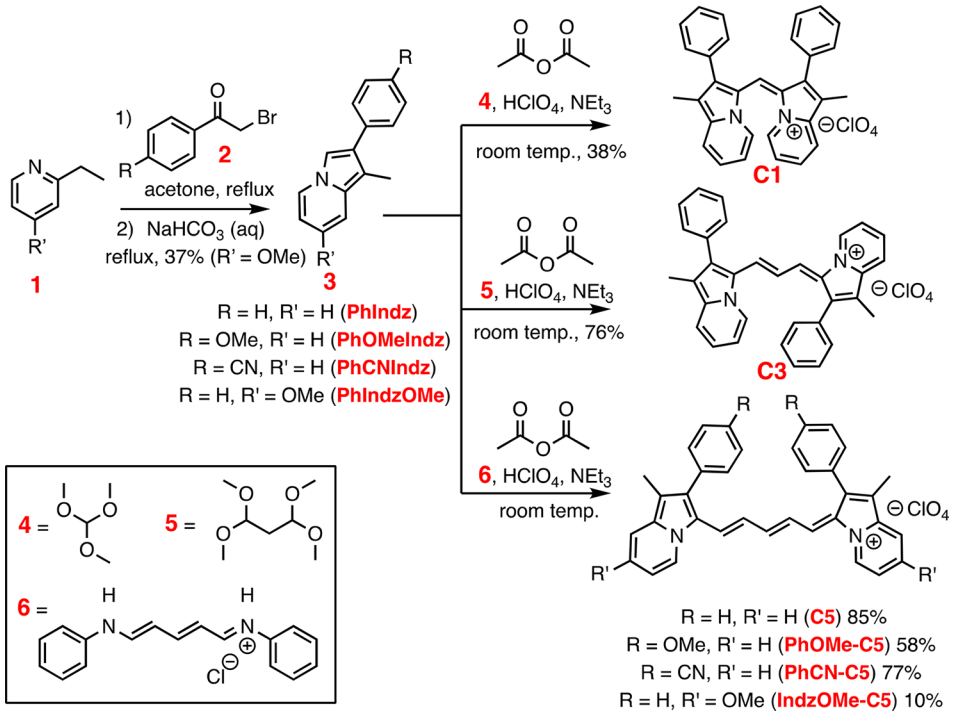

Figure 3. Synthetic route to the target indolizine cyanine dyes. The product conformations are drawn to match those obtained by crystal structure analysis of **C1**, **C3**, and **C5** (see below).

indolizines were handled with care due to limited stability, as they were found to decompose in solution under air and on silica gel; however, once the indolizine was incorporated into a cyanine dye the motif became stable to prolonged ambient exposure.

With the target dyes in hand, single-crystal X-ray diffraction studies were undertaken to probe the planarity of the dye π-system and to analyze the cyanine bridge bond lengths. We hypothesized the following: (1) **C1** potentially cannot adopt a conformation with both indolizine heterocycles coplanar due to steric interactions between the indolizine groups with the short single carbon bridge, and (2) both **C3** and **C5** require some deviation from ideal bond angles or π-system planarity due to steric interactions between the indolizine and cyanine bridge. To probe these predictions, crystals suitable for crystallographic studies were grown by slow evaporation of MeCN from **C1**, or via vapor diffusion techniques in the cases of **C3** and **C5**. The crystals grew as thin needles or granules with a metallic like orange luster, as is common for very high molar absorptivity organic materials. The resolved structures are shown below (Figure 4) with select properties reported in Table 1.

First, the planarity of each derivative was analyzed. As expected, the indolizine groups of **C1** are not coplanar and have π-systems perturbed by a 43° dihedral angle (Table 1). As a result, **C1** adopts a propeller type molecular shape, which significantly affects the molar absorptivity of this derivative (discussion below). **C3** and **C5** have lengthened methine chains that can allow for more coplanar conformations. The indolizine groups can adopt two different *cis* conformations or a *trans* type conformation with the phenyl groups either on the same side of the methine bridge or on opposite sides, respectively (see Table S4 for an illustration of the cis conformations). The *trans* conformer is the observed conformation of **C3** in the crystal structure, with a 175° dihedral angle (5° from coplanarity). Upon extending the methine chain to a five-carbon segment, the *cis* conformer was observed via crystallography, with a deviation of indolizine-indolizine π-faces from planarity by a 30° dihedral angle. The presence of both the *cis* and *trans* isomers of the indolizine cyanine dyes as crystals and the ^{1}H NMR appearing as a single set of peaks suggests that both isomers are accessible and interconversion between *cis* and *trans* isomers is likely possible

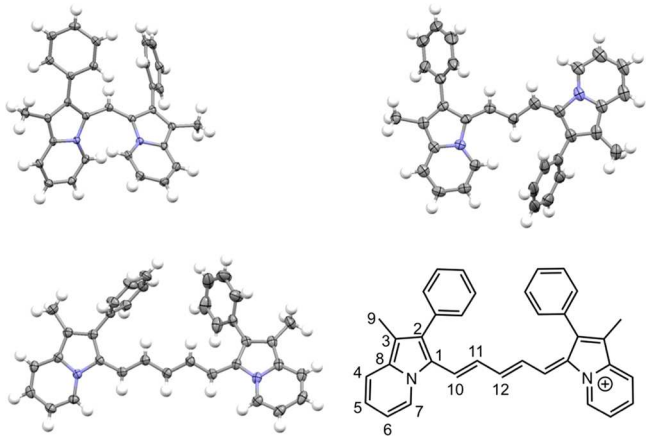

Figure 4. Crystal structures of **C1**, **C3**, and **C5** with cocrystallized solvents and counterions omitted. Hydrogens are included in order to emphasize potential steric interactions.

Table 1. Select Crystal Structure Geometry Measurements

dye	indz.-indz. dihedral (deg)	C1−C10 (Å)	C10−C11 (Å)	C11−C12 (Å)
C1	43	1.37 (1)	–	–
C3	175	1.38 (7)	1.39 (2)	–
C5	30	1.38 (3)	1.40 (2)	1.37 (5)

DOI: 10.1021/acs.joc.8b02521
J. Org. Chem. 2019, 84, 687−697

as was observed for prior squaraine derivatives.[25] Bond length analysis reveals a reasonably uniform bond length (weak alternation) when the indolizine-cyanine bond is compared to the bonds of the cyanine bridge. This bond uniformity is indicative of cyanine type structures and extends from the attachment point of the cyanine bridge to the indolizine across the π-bridge with lengths varying by less than 0.03 Å for all derivatives. The observed bond lengths (1.37−1.40 Å) are between that of an average single C−C bond (1.54 Å) and a double C−C bond (1.34 Å, Table 1). This bond length uniformity suggests these systems are more likely to exhibit $\pi-\pi^*$ optical transitions than $n-\pi^*$ optical transition and that the nonbonding electron lone pairs, which are often formally drawn on the nitrogens of the indolizine groups, are delocalized.

Absorption and emission studies were undertaken to analyze the optical properties of the dyes. First, the molar absorptivity and absorption curve features were analyzed for **C1**, **C3**, and **C5** to compare the effect of added methine spacers in several solvents (DCM, DMSO, 1:1 MeCN/H_2O, and MeCN) differing in polarity and protic nature (Figure 5, Tables 2, S1 and S2). The absorption maxima were found to shift to longer wavelength with increasing number of methine groups (e.g., in DMSO λ_{max} values 652, 705, and 819 nm are observed for **C1**, **C3**, and **C5**, respectively). These maxima are likely from $\pi-\pi^*$ transitions based on bond length alternations observed from crystallography, DFT, and the high molar absorptivity values observed (see discussion below). This is a 23−26 nm red-shift for the **C5** derivative relative to the common indoline cyanine dye, **ICG**. Additionally, the molar absorptivity increased dramatically as the cyanine bridge length increased from 1 to 3 or more carbons. The twisted π-system of **C1** prevents a strong low-energy transition, limiting molar absorptivities from 11 000 to 27 000 M^{-1} cm^{-1} for **C1** depending on solvent selection. **C3** and **C5** molar absorptivities are in stark contrast to this at up to 204 000 and 188 000 M^{-1} cm^{-1}, respectively. These values are similar to **ICG**, which has a maximum measured molar absorptivity of 238 000 M^{-1} cm^{-1}. A characteristic cyanine high-energy shoulder is observed for each of the dyes, and this is attributed to vibronic transitions.[27] Both **C3** and **C5** exhibit similar molar absorptivity trends with solvents in the following order: DCM > DMSO > MeCN/H_2O > MeCN. These trends do not correlate to dielectric constants or dipole of solvent, which indicates a subtler solvent−dye interaction is occurring to vary molar absorptivities (Table S1). **C1** follows a different molar absorptivity trend, and this deviation away from the pattern observed for **C3** and **C5** may originate from lack of planarity of the π-system of **C1**.

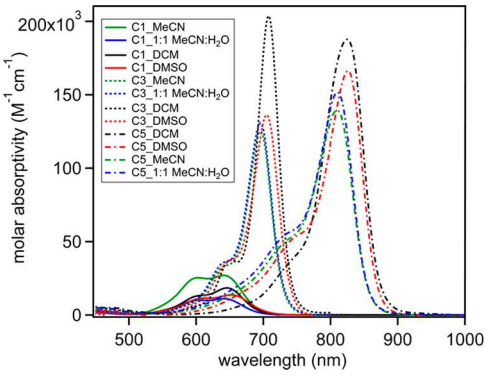

Figure 5. Molar absorptivities of **C1**, **C3**, and **C5** dyes in DCM, DMSO, MeCN, and 1:1 MeCN/H_2O measured at 1 × 10^{-5} M concentrations. See Figure S1 for the full visible range. Individual plots of the absorption and emission of **C1**, **C3**, and **C5** dyes in the four solvents are in the SI (Figures S2−S4).

A host of additional solvents were analyzed for the **C1**, **C3**, and **C5** dyes to show solvent effects on absorption wavelength (see Figures 6−8). For each solvent analyzed via absorption spectroscopy, an emission spectrum in the same solvent was analyzed. For **C1**, the solvent had a significant effect on the absorption curve shape, with the shoulder at 600 nm changing intensity relative to the lower energy peak at 650 nm (Figure 6). THF shows the closest ratio of high-energy to lower-energy features nearing equal heights, while DCM shows the high-energy feature at about a 75% of the height of the low-energy feature. All the dyes were found to have a linear absorbance versus concentration dependence following the Beer−Lambert Law from low concentrations (<1 × 10^{-6} M) to high concentrations (>1 × 10^{-5} M), which suggests the solvent dependent features in the **C1** absorption spectrum are not due to aggregation. These results show that **C1** has significantly different ground-state solution conformations depending on solvent selection. The emission curve shape variation with solvent was even more dramatic. The emission maxima could be tuned over an ∼200 nm range by solvent selection. THF and DMF represent the highest energy emission peaks near 650 nm, while DMSO, methanol, and ethanol all show peaks at wavelengths >800 nm, with DMSO being the most red-shifted at 850 nm. This is a 194 nm Stokes shift and represents a very large reorganization energy (0.43 eV) from the ground state to the excited state. All three of the solvents with the lowest energy emission spectrum peaks show dual emission behavior with an emission peak near 700 nm. This type of dichromic behavior has been observed previously with nonsymmetric cyanine dyes.[29] The low-energy emission is the dominant feature in MeOH, while the high-energy emission is dominant in DMSO. The remaining solvents all show a peak near 700 nm and typically show a shoulder at 750 nm, which mirrors the absorption spectrum, suggesting the higher energy absorption feature is vibronic in nature. The vast range of emission curve shapes and peak energies suggests a wide range of geometries are accessible in the excited state and the excited-state geometry is exceptionally solvent dependent. The quantum yield for **C1** was measured to be less than 1% in the same four solvents as the molar absorptivity studies (Table 2). This leads to a low molecular brightness upper limit of ≤300, as is expected from a molecule with a very large reorganization energy.

For the absorption curve profiles of **C3** and **C5**, solvent effects are not as dramatic as with **C1** (Figures 7 and 8). **C3** and **C5** show typical cyanine curve shapes with little energetic variation in the absorption curve maxima based on solvent choice (<20 nm change observed in the 12 solvents examined). The emission curves show a slight increase in solvent effect changes with a range of about 35 nm observed for **C3** and **C5**. Notably, the most red-shifted and most blue-shifted solvents change between these two derivatives, suggesting subtle differences in solvent interactions between these two dyes. Stokes shifts between 30 and 50 nm were observed for these dyes, which allows for use in some biological imaging applications.[30] Both **C3** and **C5** show >1% quantum yields with the highest values (1.6% and 3.5%, respectively) observed

DOI: 10.1021/acs.joc.8b02521
J. Org. Chem. 2019, 84, 687−697

Table 2. Molar Absorptivity, Absorption Maximum, Emission Maximum, Quantum Yield, and Stokes Shift for Each Dye in Four Solvents[a]

dye	solvent	ε (M^{-1} cm^{-1})	λ_{max}^{abs} (nm)	λ_{max}^{emis} (nm)	Φ (%)	MB ($\varepsilon \times \Phi$)	Stokes shift (nm | eV | cm^{-1})
C1	MeCN	27 000	642	698	<1	≤300	56 | 0.15 | 1250
	1:1 MeCN/H_2O	11 000	641	698	<1	≤100	57 | 0.16 | 1270
	DMSO	14 000	652	846	<1	≤100	194 | 0.43 | 3517[b]
	DCM	18 000	646	693	<1	≤200	47 | 0.13 | 1050
C3	MeCN	126 000	695	725	<1	≤1300	30 | 0.07 | 595
	1:1 MeCN/H_2O	133 000	696	727	<1	≤1300	31 | 0.08 | 613
	DMSO	135 000	705	737	1.6	2200	32 | 0.08 | 616
	DCM	204 000	708	741	<1	≤2000	33 | 0.08 | 629
C5	MeCN	140 000	810	848	1.2	1700	38 | 0.07 | 553
	1:1 MeCN/H_2O	151 000	811	840	<1	≤1500	29 | 0.05 | 426
	DMSO	166 000	819	852	3.5	5800	33 | 0.06 | 473
	DCM	188 000	825	868	2.2	4100	43 | 0.07 | 600
PhOMe-C5	MeCN	94 000	799	845	1.3	1200	46 | 0.08 | 681
	1:1 MeCN/H_2O	146 000	799	831	<1	≤1500	32 | 0.06 | 482
	DMSO	162 000	816	840	2.7	4400	24 | 0.04 | 350
	DCM	207 000	813	863	1.9	3900	50 | 0.09 | 713
PhCN-C5	MeCN	122 000	799	854	<1	≤1200	55 | 0.10 | 806
	1:1 MeCN/H_2O	100 000	805	851	<1	≤1000	46 | 0.08 | 671
	DMSO	84 000	820	860	2.3	1900	40 | 0.07 | 567
	DCM	151 000	812	870	2.0	3000	58 | 0.10 | 821
IndzOMe-C5	MeCN	124 000	819	849	1.3	1600	30 | 0.05 | 431
	1:1 MeCN/H_2O	138 000	821	859	<1	≤1400	38 | 0.07 | 539
	DMSO	141 000	838	868	3.6	5100	30 | 0.05 | 412
	DCM	151 000	823	876	<1	<1500	53 | 0.09 | 735
ICG	1:1 MeCN/H_2O	238 000	785	816	9.1	21 700	31 | 0.06 | 484
	DMSO	211 000	797	835	17.1	36 100	38 | 0.07 | 571
$PhIn_2SQ$	DCM	181 000	716	766	2.1	3800	50 | 0.11 | 912
bis-t-$buPhIn_2SQ$	DCM	216 000	716	736	9.5	20 500	20 | 0.05 | 380
$TTD(T)_2$	Toluene	12 000	624	765	16.8	2000	141 | 0.37 | 2954
TPA-BBTD-TPA	Toluene	24 000	763	1065	7.1	1700	302 | 0.46 | 3716
CH1055-PEG	H_2O	–	750	1055	0.3	–	305 | 0.48 | 3855

[a]Absorption and emission curves for **PhOMe-C5**, **PhCN-C5**, and **PhIndzOMe-C5** are in the SI (Figures S5–S7). Data for **ICG** were collected under identical conditions as a benchmark. Data for $PhIn_2SQ$,[25] *bis-t*-$buPhIn_2SQ$,[25] $TTD(T)_2$,[24] TPA-BBTD-TPA,[28] and CH1055-PEG[10] are from literature reports. ε is molar absorptivity. λ_{max}^{abs} is the absorption curve low energy peak value. λ_{max}^{emis} is the emission curve peak value. Φ is the quantum yield. MB is molecular brightness. [b]This value is based on the smaller lower energy emission peak. A higher energy emission peak (715 nm) is also observed which would correspond to a Stokes shift of 63 nm, 0.17 eV.

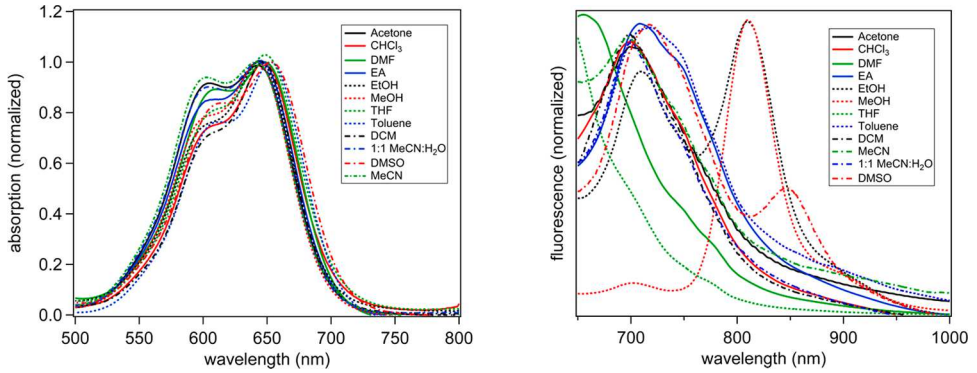

Figure 6. Absorption (left) and emission (right, fit with 0.1 LOESS function) spectra of **C1** in various solvents. Absorption spectra were collected at 1×10^{-5} M. Emission spectra were collected with excitation at 633 nm.

in DMSO. A high MB value of 5800 is observed for **C5**. While the MB values for the indolizine-cyanine dyes were not as high as those reported for the ICG benchmark, it should be noted that these values can be improved dramatically through enhancing the emission quantum yield by selection of nonconjugated substituents, as was recently shown for CH1055-PEG.[15] Compared to other benchmark materials such as D–A–D dyes based on squaraine ($PhIn_2SQ$ and *bis-t*-$buPhIn_2SQ$) and thienothiadiazole ($TTD(T)_2$), **C5** is significantly more red-shifted by >100 nm in absorption and emission spectrum maxima. The reorganization energy of **C5** is similar to that of the squaraine derivatives, which have large

DOI: 10.1021/acs.joc.8b02521
J. Org. Chem. 2019, 84, 687–697

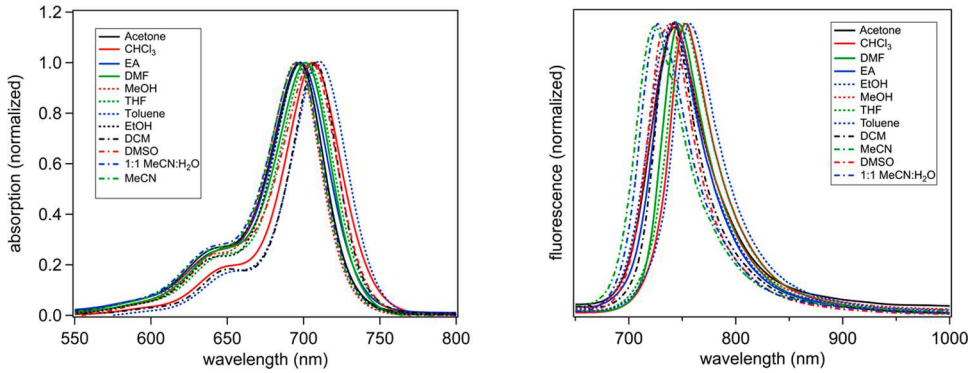

Figure 7. Absorption (left) and emission (right, fit with 0.1 LOESS function) spectra of **C3** in various solvents. Absorption spectra were collected at 1×10^{-5} M. Emission spectra were collected with excitation at 633 nm.

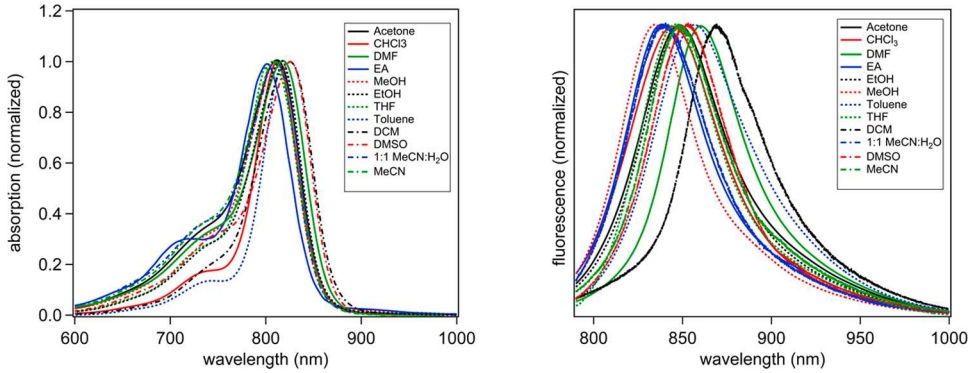

Figure 8. Absorption (left) and emission (right, fit with 0.1 LOESS function) spectra of **C5** in various solvents. Absorption spectra were collected at 1×10^{-5} M. Emission spectra were collected with excitation at 785 nm.

Stokes shifts for that class of materials (0.07 eV versus 0.05–0.11 eV). Despite being red-shifted significantly with a larger Stokes shift, the MB of **C5** is higher than these comparison dyes even with the very high quantum yield of $TTD(T)_2$. Compared to one of the most red-shifted imaging materials, TPA-BBTD-TPA (and derivative CH1055-PEG), a significantly higher MB is observed for **C5** with a more red-shifted absorption maximum. Notably, a significantly more red-shifted emission is present with TPA-BBTD-TPA. Overall, compared to the benchmark materials analyzed, **C5** is a promising dye scaffold for future applications.

The remaining indolizine-cyanine dyes synthesized are analogues of **C5** and show comparable absorption maxima, emission maxima, quantum yields, and MB to the parent compound in most solvents (Figures S4–S6). These derivatives (**PhOMe-C5**, **PhCN-C5**, and **IndzOMe-C5**) are dramatically different in substituent electronic nature with **PhOMe-C5** and **IndzOMe-C5** having a strong electron donating OMe group and **PhCN-C5** having a strong electron withdrawing group. The lack of change in the absorption and emission spectrum suggests these derivatives do not have a strong effect on the π-conjugated system (see computational discussion below). These positions on the indolizine heterocycle and phenyl group of the indolizine have little effect on the optical properties of these dyes and are attractive positions for functionalization to introduce components such as water solubilizing groups or bioconjugation functionality. The **C5** derivatives show up to a 41 nm red shift relative to **ICG** in DMSO, indicating a deeper NIR light absorption as is desired for many applications (Figures S8 and S9). This red shift occurs despite a two methine shorter bridge for the C5 indolizine cyanine derivatives.

To better understand the role of the indolizine group and the optical properties of these dyes, calculations were performed using density functional theory (DFT) at the M06-2X/6-311G(d,p) level with the Gaussian 16 software package.[31,32] The SMD solvation model was used during geometry optimizations to better approximate the presence of MeCN.[33] Both the *cis* and *trans* isomers were analyzed since crystallography revealed the presence of *cis* isomers for **C1** and **C5** but the *trans* isomer of **C3**. A small energy difference was found between the ground state geometries of 1.0–4.4 kcal/mol with the *trans* isomer slightly lower in energy for **C1** and one of the *cis* isomers slightly lower in energy for **C3** and **C5** (see Supporting Information). For all derivatives studied the highest occupied molecular orbital (HOMO) and lowest unoccupied molecular orbital (LUMO) were delocalized across the entire π-system, with significant orbital presence on both the methine bridge and on the indolizine donors (Figures 9 and S16). It is noteworthy that the HOMO and LUMO are extended onto the conjugated indolizine heterocycle to a greater extent than is observed in the case of indoline cyanines.[34] This suggests the indolizine cyanine dyes may be electronically tuned more effectively than with indoline cyanines by careful substitution on the indolizine donor group.

For comparison to experimental trends, time dependent (TD)-DFT calculations were carried out at the same level of theory as the geometry optimizations (Table 3). TD-DFT shows a similar trend to the observed experimental data for the *cis* isomer with a close C7–C11 interaction for both λ_{max} and ε when compared with the vertical transition energies and

DOI: 10.1021/acs.joc.8b02521
J. Org. Chem. 2019, 84, 687–697

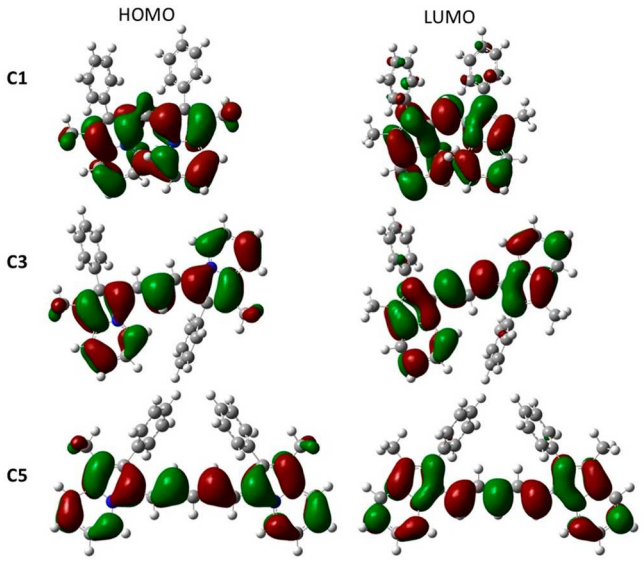

Figure 9. HOMO and LUMO images for **C1**, **C3**, and **C5** with an isovalue of 0.02.

Table 3. TD-DFT Values for the Ground- and Excited-State Optimized Geometries

dye	vertical trans. (eV, nm)	oscillator strength	dye* vertical trans. (eV, nm)	osc. str. dye*	Stokes shift (eV, nm)
C1 *cis*[a]	2.20, 561	0.79	1.78, 697	0.47	0.42, 136
C3 *trans*[a]	2.33, 533	1.11	2.18, 569	0.97	0.15, 36
C3 *cis*[b]	1.91, 648	1.49	1.74, 712	1.27	0.17, 64
C5 *cis*[b]	1.65, 752	2.06	1.51, 822	1.84	0.14, 70
C5 *cis*[a,c]	2.08, 596	1.52	2.03, 611	1.75	0.05, 15

[a]Conformation observed by crystallography. [b]C7−C11 interaction in Figure 1. [c]C7−C10 interaction in Figure 1.

oscillator strengths in MeCN: **C1** < **C3** < **C5** (Table 3, Figure 1). When the different conformers obtained from the crystal structure analysis are compared computationally, **C1** is red-shifted relative to **C3**, and the energy of the vertical transition is significantly different than the experimental absorption spectrum maximum. As an example comparison, **C5** with the C7−C11 close interaction *cis* conformer shows theory and solution experiments within 0.12 eV. When the conformer observed via crystallography is computationally analyzed, the comparison with solution experimentation shows a larger variation of 0.55 eV. We note that the energy difference between these geometries is small at 2 kcal/mol, and since ^{1}H NMR shows only a single isomer, rapid interconversion is likely possible. These transitions were found to be HOMO to LUMO $\pi-\pi^*$ transitions. To analyze the experimental emission spectrum data computationally, the excited-state geometry for each derivative was optimized. Similar to experimental data, **C5** was found to have the most red-shifted excited-state geometry vertical transition (labeled dye* vertical trans. in Table 3) and strongest oscillator strength (brightest emission). **C1** was computationally shown to have the largest Stokes shift, which is in good agreement with experimental data. Electron density difference mapping of the three dyes was used to show where electrons are traveling from (red) and to (blue) upon photoexcitation (Figures 10 and S17). Green areas represent minimal electron movement. The maps show a

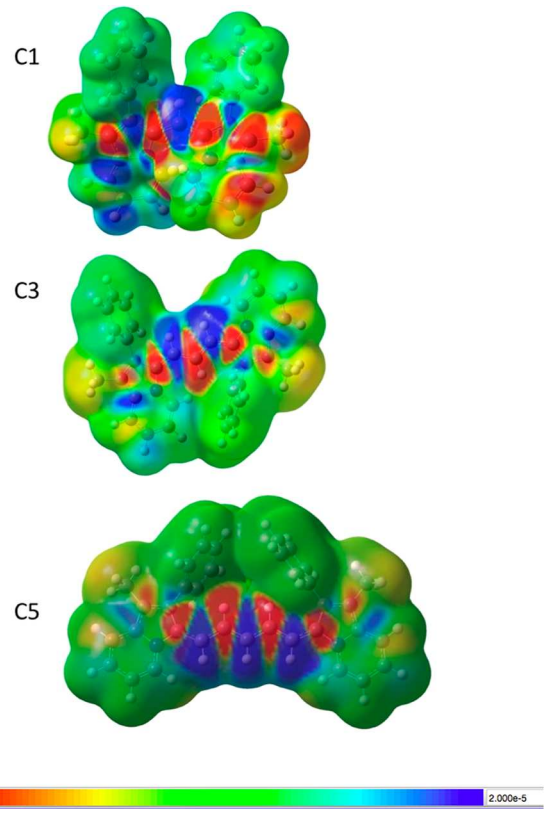

Figure 10. Electron density difference map. Red is where electrons originate from, blue is where they travel to upon photoexcitation, and green is neutral.

delocalization of electron density across the cyanine π-bridge extending onto the full indolizine π-system in red, and a similar delocalization of areas accepting electron density on alternating atoms. No significant contribution from the phenyl group is observed on the electron density difference maps.

The predicted geometry changes from the ground state to the excited state were analyzed to determine the origin of the Stokes shift in these dyes. The ground state geometry shows a deviation of bond angles from ideal 120° sp^2 hybridized bond angles to wider values for all isomers (122°−134° for the first two angles measured, Tables 4 and S3). This deviation is presumably to lower steric interactions between hydrogen atoms on the indolizine and cyanine bridge (or between the two indolizines for the case of **C1**). Despite the bond angle distortion, the nearest hydrogens are still well within a typical hydrogen bond distance (1.5−2.5 Å). Upon photoexcitation, the bond angles adopt a closer to ideal geometry at 122°−130°. These angles favor increased steric interactions between hydrogen atoms on indolizine and the cyanine bridge if the π-system were to remain planar. To relieve this increased strain, the indolizine−cyanine dihedral angle increases in the excited state by 4°−18° for all the conformers of **C3** and **C5** derivatives from nearer to planar in the ground state. This results in a less planar π-system, but does release steric strain, as evidenced by an increase in distance between nearest neighboring hydrogens of about 0.1 Å (Table S4). Thus, the ground state geometry favors bond angle distortion with a more ideal dihedral angle across the π-system, while the excited state geometry favors a distorted dihedral angle across the π-system but gains more ideal bond angles (Figure 11). This change in geometry explains the increased Stokes shift for

DOI: 10.1021/acs.joc.8b02521
J. Org. Chem. 2019, 84, 687−697

Table 4. Select Computed Bond Angles, Dihedral Angles, and Atom−Atom Distances[a]

dye	angle 1 (deg) GS | ES	angle 2 (deg) GS | ES	angle 3 (deg) GS | ES	angle 4 (deg) GS | ES	dihedral (deg) indz-cyanine GS | ES	dihedral (deg) indz−indz GS | ES	H−H bond distance (Å) GS | ES
C1	128 | 123	134 | 125	N/A	N/A	15 | 27	35 | 50	2.7 | 3.6[b]
C3	128, 123 | 127, 122	131, 126 | 129, 123	120 | 123	N/A	2, 10 | 11, 22	15 | 32	1.8, 2.1 | 1.9, 2.1
C5	122 | 122	127 | 126	122 | 124	123 | 121	7 | 11	22 | 33	2.1 | 2.0

[a]GS is ground state. ES is excited state. [b]Indicates H−H bond distance is between the two closest hydrogens of the indolizines. The structure below illustrates the bond angles being analyzed.

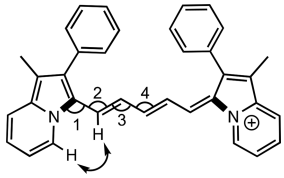

these indolizine cyanine derivatives relative to well-established indoline cyanines.

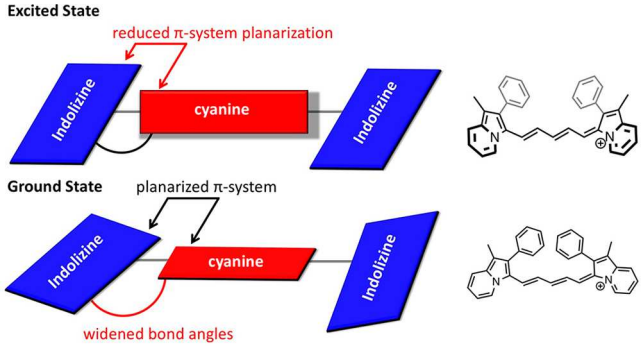

Figure 11. Illustration of geometry changes from the ground state to the excited state.

CONCLUSIONS

Six NIR indolizine-cyanine dyes were designed, synthesized, and characterized. UV−vis−NIR absorption measurements show that increasing the methine bridge lengths leads to red-shifted absorptions. The indolizine-cyanine dyes show a red-shifted absorption relative to benchmark **ICG** despite two fewer methines. This shows the critical role the indolizine groups can play in shifting absorption spectra as a conjugated donor group. The dyes were found to emit in the NIR region with the sterically congested dye **C1** showing the largest solvent effects and reorganization energies. The five methine group bridge of **C5** was found to lead to the largest quantum yields and a high MB value for a dye emitting near 900 nm. Computational studies reveal that the ground state favors a planarized π-system with distorted bond angles while the excited state favors the opposite geometry. Importantly, the use of molecularly engineered steric interactions shows that significant Stokes shifts can be designed into a class of molecules known for minimal Stokes shifts while keeping a good quantum yield and red shifting the absorption and emission curves.

EXPERIMENTAL SECTION

General Information. All commercially obtained reagents and solvents were used as received without further purification. ***Caution:*** It should be noted that the dyes were isolated as perchlorate salts, and perchlorate salts in general have been found to be explosive in some cases. Care is advised while handling all perchlorate salts. Thin-layer chromatography (TLC) was conducted with Sorbtech silica XHL TLC glass backed plates and visualized with UV. Flash column chromatography was performed using a CombiFlash Rf+ system. RediSep cartridges were charged with silica gel from Sobent Tech P60, 40−63 μm (230−400 mesh). ^{1}H and ^{13}C NMR spectra were recorded on a Bruker Avance-300 (300 MHz) spectrometer and a Bruker Avance-500 (500 MHz) spectrometer and are reported in ppm using solvent as an internal standard (DMSO at 2.50 ppm). Data are reported as s = singlet, d = doublet, t = triplet, q = quartet, p = pentet, m = multiplet, b = broad, ap = apparent, dd = doublet of doublets; coupling constant(s) are in Hz; integration. UV−vis spectra were measured with a Cary 5000 UV−vis−NIR spectrometer. HRMS spectra were obtained with a QTOF HRMS utilizing nanospray ionization. The mass analyzer was set to the 200−2000 Da range. Infrared spectra were recorded with an Agilent Cary 660 ATR-FTIR. For all derivatives, the excited-state lifetimes were found to be shorter than the response function of the instrument. The emission of the **C1** and **C3** derivatives were measured using a Horiba LabRam spectrometer with a 600 grooves/mm grating, CCD camera detection, and an excitation laser of 633 nm. All other dyes were measured using the same instrument and a 785 nm excitation laser. The quantum efficiency of the detector was accounted for when measuring emission profiles. The relative quantum yields were obtained using this equation:

$$\Phi_{\text{Sample}} = \Phi_{\text{Standard}} \cdot \frac{E_{\text{Sample}}}{E_{\text{Standard}}} \cdot \frac{A_{\text{Standard}}}{A_{\text{Sample}}} \cdot \frac{\eta^2_{\text{Sample}}}{\eta^2_{\text{Standard}}}$$

For the equation above, E is the sum of emission intensities and A is maximum absorbance. η is the refractive index of the solvent used, and Φ denotes the quantum yield.[35] The standard used to obtain the relative quantum yields was Indocyanine Green (ICG) with a quantum yield of 14% in H_2O.[36] Diffraction data were collected at 90 K on a Bruker D8 Venture dual microsource diffractometer using Mo Kα X-rays. Data scaling, merging, and absorption correction used well-established procedures.[37,38] Crystal structures were solved and refined using the Shelx programs.[39,40] Crystals of **C3** included some poorly defined solvent that was accounted for using SQUEEZE.[41]

*(Z)-1-Methyl-3-((1-methyl-2-phenylindolizin-3-yl)methylene)-2-phenyl-3H-indolizin-4-ium Perchlorate (**C1**).* To a round-bottom flask equipped with a stir bar, **PhIndz** (1.00 g, 4.80 mmol) was added to acetic anhydride (48 mL) followed by perchloric acid (0.48 g, 4.80 mmol). The mixture was allowed to stir at room temperature for 5 min. Triethylorthoformate (**4**) (0.36 g, 2.40 mmol) was added along with triethylamine (0.58 g, 5.76 mmol). The reaction mixture was allowed to stir at room temperature for 24 h before being subjected to a silica gel column with a solvent gradient beginning with 40:60 dichloromethane/hexane and ending with 100% dichloromethane. The product was isolated as a red solid (0.48 g, 38%). ^{1}H NMR (300 MHz, DMSO-d6) δ 8.50 (s, 2H), 8.08−7.97 (m, 4H), 7.90−7.80 (m,

DOI: 10.1021/acs.joc.8b02521
J. Org. Chem. 2019, 84, 687−697

4H), 7.44−7.37 (m, 8H), 7.3 (t, J = 6.8 Hz, 1H), 2.38 (s, 6H). ^{13}C NMR was not obtained due to low solubility. IR (neat, cm^{-1}): 3598, 3534, 2916, 2665, 2329, 2092, 1777, 1621, 1586, 1464. HRMS m/z calculated for $C_{31}H_{25}N_2$ [M − ClO_4]$^+$: 425.2018, found 425.2019. Melting point: 157−162 °C.

*(Z)-1-Methyl-3-((E)-3-(1-methyl-2-phenylindolizin-3-yl)-allylidene)-2-phenyl-3H-indolizin-4-ium Perchlorate (**C3**).* To a round-bottom flask equipped with a stir bar, **PhIndz** (0.35 g, 1.69 mmol) was added to acetic anhydride (17.0 mL) followed by perchloric acid (0.169 g, 1.69 mmol). The mixture was allowed to stir at room temperature for 5 min. Malonaldehyde bis(dimethyl acetal) (**5**) (0.139 g, 0.845 mmol) was added along with triethylamine (0.205 g, 2.03 mmol). The reaction mixture was allowed to stir at room temperature for 24 h before being subjected to a silica gel column with a solvent gradient beginning with a 50:50 dichloromethane/hexane solvent mixture and ending with 100% dichloromethane. The product was isolated as a gold solid (0.35 g, 76%). ^{1}H NMR (300 MHz, DMSO-d6) δ 7.99 (d, J = 8.5 Hz, 2H), 7.76−7.68 (m, 9H), 7.46−7.31 (m, 9H), 6.69 (t, J = 13.2 Hz, 1H), 2.19 (s, 6H). ^{13}C NMR was not obtained due to sparing solubility. IR (neat, cm^{-1}): 3109, 2993, 2817, 2669, 2582, 2330, 2116, 1618, 1555, 1533, 1454. HRMS m/z calculated for $C_{33}H_{27}N_2$ [M + H]$^+$: 451.2174, found 451.2197. Melting point (dec.): 252−253 °C.

*(Z)-1-Methyl-3-((2E,4E)-5-(1-methyl-2-phenylindolizin-3-yl)-penta-2,4-dien-1-ylidene)-2-phenyl-3H-indolizin-4-ium Perchlorate (**C5**).* To a round-bottom flask equipped with a stir bar, **PhIndz** (1.00 g, 4.80 mmol) was added to acetic anhydride (48.0 mL) followed by perchloric acid (0.48 g, 4.80 mmol). The mixture was allowed to stir at room temperature for 5 min. (Phenylamino)pentadienylidene aniline HCl (**6**) (0.68 g, 2.40 mmol) was added along with triethylamine (0.58 g, 5.76 mmol). The reaction mixture was allowed to stir at room temperature for 24 h before being subjected to a silica gel column with a solvent gradient beginning at 50:50 dichloromethane/hexane and ending with 100% dichloromethane. The product was isolated as a gold solid (1.1 g, 82%). ^{1}H NMR (300 MHz, DMSO-d6) δ 9.18 (d, J = 6.9 Hz, 2H), 8.03 (d, J = 13.6 Hz, 2H), 7.91 (d, J = 8.6 Hz, 2H), 7.70−7.54 (m, 8H), 7.37−7.25 (m, 8H), 5.91 (t, J = 12.5 Hz, 1H), 2.14 (s, 6H). ^{13}C NMR was not obtained due to sparing solubility. IR (neat, cm^{-1}): 3652, 2670, 2564, 2329, 2116, 1925, 1806, 1671, 1617, 1516, 1458. HRMS m/z calculated for $C_{35}H_{29}N_2$ [M]$^+$: 477.2331, found 477.2315. Melting point (dec.): 176−179 °C.

*(Z)-2-(4-Methoxyphenyl)-3-((2E,4E)-5-(2-(4-methoxyphenyl)-1-methylindolizin-3-yl)penta-2,4-dien-1-ylidene)-1-methyl-3H-indolizin-4-ium Perchlorate (**PhOMe-C5**).* To a round-bottom flask equipped with a stir bar, **PhOMeIndz** (1.08 g, 4.54 mmol) was added to acetic anhydride (45.0 mL) followed by perchloric acid (0.46 g, 4.54 mmol). The mixture was allowed to stir at room temperature for 5 min. (Phenylamino)pentadienylidene aniline HCl (**6**) (0.65 g, 2.27 mmol) was added along with triethylamine (0.55 g, 5.45 mmol). The reaction mixture was allowed to stir at room temperature for 24 h before being poured into ether (200 mL). The pure product was insoluble in ether and was isolated by vacuum filtration as a red solid (0.81 g, 58%). ^{1}H NMR (300 MHz, DMSO-d6) δ 9.16 (d, J = 6.9 Hz, 2H), 7.90−7.85 (m, 2H), 7.70 (t, J = 15.6 Hz, 2H), 7.45−7.29 (m, 8H), 7.13 (d, J = 8.3 Hz, 6H), 6.42 (t, J = 11.5 Hz, 1H), 3.91 (s, 6H), 2.14 (s, 6H). ^{13}C NMR was not obtained due to sparing solubility. IR (neat, cm^{-1}): 3656, 3581, 3333, 2831, 2656, 2463, 2329, 2116, 1919, 1804, 1754, 1706, 1658, 1607, 1555, 1516, 1465. HRMS m/z calculated for $C_{37}H_{33}N_2O_2$ [M]$^+$: 537.2542, found 537.2516. Melting point (dec.): 158−161 °C.

*(Z)-2-(4-Cyanophenyl)-3-((2E,4E)-5-(2-(4-cyanophenyl)-1-methylindolizin-3-yl)penta-2,4-dien-1-ylidene)-1-methyl-3H-indolizin-4-ium Perchlorate (**PhCN-C5**).* To a round-bottom flask equipped with a stir bar, **PhCNIndz** (1.00 g, 4.31 mmol) was added to acetic anhydride (45.0 mL) followed by perchloric acid (0.432 g, 4.31 mmol). The mixture was allowed to stir at room temperature for 5 min. (Phenylamino)pentadienylidene aniline HCl (**6**) (0.613 g, 2.15 mmol) was added along with triethylamine (0.523 g, 5.17 mmol). The reaction mixture was allowed to stir at room temperature for 24 h before being poured into ether (200 mL). The pure product was insoluble in ether and was isolated by vacuum filtration as a red solid (1.0 g, 77%). ^{1}H NMR (300 MHz, DMSO-d6) δ 9.19 (d, J = 6.8 Hz, 2H), 8.05 (d, J = 8.1 Hz, 4H), 7.98 (d, J = 8.6 Hz, 2H), 7.91 (d, J = 14.0 Hz, 2H), 7.76 (t, J = 7.6 Hz, 2H), 7.65 (d, J = 8.1 Hz, 4H), 7.44−7.36 (m, 4H), 6.21 (t, J = 13.2 Hz, 1H), 2.18 (s, 6H). ^{13}C NMR was not obtained due to sparing solubility. IR (neat, cm^{-1}): 3611, 3395, 2354, 2332, 2116, 1619, 1612, 1530, 1527, 1471. HRMS m/z calculated for $C_{37}H_{27}N_4$ [M]$^+$: 527.2236, found 527.2251. Melting point (dec.): 187−191 °C.

*(Z)-1-Methyl-3-((E)-3-(1-methyl-2-phenylindolizin-3-yl)-allylidene)-2-phenyl-3H-indolizin-4-ium Perchlorate (**IndzOMe-C5**): Part 1: 7-Methoxy-1-methyl-2-phenylindolizine (**4**, **PhIndzOMe**).* To a round-bottom flask equipped with a stir bar and a reflux condenser were added 2-ethyl-4-methoxypyridine (0.39 g, 2.81 mmol) and bromoacetophenone (0.84 g, 4.22 mmol) in acetone (5.62 mL). The mixture was heated to reflux in an oil bath for 24 h. The reaction was monitored by TLC. Upon disappearance of the starting material **2**, water (5.62 mL) and sodium bicarbonate (0.94 g, 11.2 mmol) were added to the reaction mixture. The mixture was heated at reflux in an oil bath for 2 h. The crude product oiled out of solution and was extracted with dichloromethane to yield a brown oil that was immediately subjected to a rapid plug filtration through silica gel with 20:80 ethyl acetate/hexanes to yield an off-white solid. Due to oxidative instability, the intermediate was carried forward to the next reaction without any further purification or characterization. To a round-bottom flask equipped with a stir bar under nitrogen, the intermediate PhIndzOMe (0.25 g, 1.05 mmol) was added to acetic anhydride (10.5 mL) followed by perchloric acid (0.11 g, 1.05 mmol). The mixture was allowed to stir at room temperature for 5 min. (Phenylamino)pentadienylidene aniline HCl (**6**) (0.15 g, 0.52 mmol) was added along with triethylamine (0.13 g, 1.26 mmol). The reaction mixture was allowed to stir at room temperature for 3 h before being subjected to a plug of silica with a solvent gradient from 100% dichloromethane to 50:50 ethyl acetate/dichloromethane. A final purification was performed by dissolving the concentrated product in a minimal amount of dichloromethane followed by the addition of diethyl ether/hexanes (50:50) to yield the pure product as a green solid (0.03 g, 10%). ^{1}H NMR (300 MHz, DMSO-d6) δ 9.02 (d, J = 7.5 Hz, 2H), 7.73−7.53 (m, 10H), 7.33 (d, J = 7.2 Hz, 4H), 7.15−7.01 (m, 4H), 5.86 (t, J = 14.4 Hz, 1H), 4.01 (s, 6H), 2.10 (s, 6H). ^{13}C NMR was not obtained due to sparing solubility. IR (neat, cm^{-1}): 3788, 3691, 2917, 2633, 2329, 2116, 1797, 1775, 1630, 1527, 1444. HRMS m/z calculated for $C_{37}H_{33}N_2O_2$ [M]$^+$: 537.2542, found 537.2532. Melting point (dec.): 162−165 °C.

■ ASSOCIATED CONTENT

Supporting Information

The Supporting Information is available free of charge on the ACS Publications website at DOI: 10.1021/acs.joc.8b02521.

Crystallographic data for **C1** (CIF)

Crystallographic data for **C3** (CIF)

Crystallographic data for **C5** (CIF)

Table of dielectric constants, dye solubility table, additional absorption and emission plots, NMR spectra, HOMO−LUMO diagrams, electron density difference maps, calculated XYZ coordinates, additional crystallography data (PDF)

■ AUTHOR INFORMATION

Corresponding Author

*E-mail: delcamp@olemiss.edu.

ORCID

Jacqueline Gayton: 0000-0002-3564-1663

Shane A. Autry: 0000-0002-6872-7885

William Meador: 0000-0002-9869-026X

DOI: 10.1021/acs.joc.8b02521
J. Org. Chem. 2019, 84, 687−697

Sean R. Parkin: 0000-0001-5777-3918
Nathan I. Hammer: 0000-0002-6221-2709
Jared H. Delcamp: 0000-0001-5313-4078

Author Contributions

[‖]J.G. and S.A.A. contributed equally.

Notes

The authors declare no competing financial interest.

■ ACKNOWLEDGMENTS

The D8 Venture diffractometer at the University of Kentucky was funded by the NSF (MRI CHE-1625732). The Horiba LabRam spectrometer at the University of Mississippi was funded by the NSF (MRI CHE-1532079). J.N.G., W.M., G.H., and J.H.D. thank the NSF for Award OIA-1632825. S.A. and N.I.H. thank the NSF for Award OIA-1539035.

■ REFERENCES

(1) Shindy, H. A. Fundamentals in the Chemistry of Cyanine Dyes: A Review. *Dyes Pigm.* **2017**, *145*, 505−513.
(2) Xue, J.; Li, C.; Xin, L.; Duan, L.; Qiao, J. High-Efficiency and Low Efficiency Roll-Off Near-Infrared Fluorescent OLEDs through Triplet Fusion. *Chem. Sci.* **2016**, *7*, 2888−2895.
(3) Tuong Ly, K.; Chen-Cheng, R.-W.; Lin, H.-W.; Shiau, Y.-J.; Liu, S.-H.; Chou, P.-T.; Tsao, C.-S.; Huang, Y.-C.; Chi, Y. Near-Infrared Organic Light-Emitting Diodes with Very High External Quantum Efficiency and Radiance. *Nat. Photonics* **2017**, *11*, 63−68.
(4) Suzuki, H. Organic Light-Emitting Materials and Devices for Optical Communicaiton Technology. *J. Photochem. Photobiol., A* **2004**, *166*, 155−161.
(5) Yang, Z.; Sharma, A.; Qi, J.; Peng, X.; Lee, D. Y.; Hu, R.; Lin, D.; Qu, J.; Kim, J. S. Super-Resolution Fluorescent Materials: An Insight into Design and Bioimaging Applications. *Chem. Soc. Rev.* **2016**, *45*, 4651−4667.
(6) Keereweer, S.; Van Driel, P. B. A. A.; Snoeks, T. J. A.; Kerrebijn, J. D. F.; Baatenburg de Jong, R. J.; Vahrmeijer, A. L.; Sterenborg, H. J. C. M.; Löwik, C. W. G. M. Optical Image-Guided Cancer Surgery: Challenges and Limitations. *Clin. Cancer Res.* **2013**, *19*, 3745−3754.
(7) Escobedo, J. O.; Rusin, O.; Lim, S.; Strongin, R. M. NIR Dyes for Bioimaging Applications. *Curr. Opin. Chem. Biol.* **2010**, *14*, 64−70.
(8) Bricks, J. L.; Slominskii, Y. L.; Panas, I. D.; Demchenko, A. P. Fluorescent J-Aggregates of Cyanine Dyes: Basic Research and Applications Review. *Methods Appl. Fluoresc.* **2018**, *6*, 012001.
(9) Shi, C.; Wu, J. B.; Pan, D. Review on near-Infrared Heptamethine Cyanine Dyes as Theranostic Agents for Tumor Imaging, Targeting, and Photodynamic Therapy. *J. Biomed. Opt.* **2016**, *21*, 50901.
(10) Antaris, A. L.; Chen, H.; Cheng, K.; Sun, Y.; Hong, G.; Qu, C.; Diao, S.; Deng, Z.; Hu, X.; Zhang, B.; Zhang, X.; Yaghi, O. K.; Alamparambil, Z. R.; Hong, X.; Cheng, Z.; Dai, H. A Small-Molecule Dye for NIR-II Imaging. *Nat. Mater.* **2016**, *15*, 235−242.
(11) Peng, X.; Song, F.; Lu, E.; Wang, Y.; Zhou, W.; Fan, J.; Gao, Y. Heptamethine Cyanine Dyes with a Large Stokes Shift and Strong Fluorescence: A Paradigm for Excited-State Intramolecular Charge Transfer. *J. Am. Chem. Soc.* **2005**, *127*, 4170−4171.
(12) Han, J.; Engler, A.; Qi, J.; Tung, C. H. Ultra Pseudo-Stokes Shift near Infrared Dyes Based on Energy Transfer. *Tetrahedron Lett.* **2013**, *54*, 502−505.
(13) Smith, A. M.; Mancini, M. C.; Nie, S. Bioimaging: Second Window for in Vivo Imaging. *Nat. Nanotechnol.* **2009**, *4*, 710−711.
(14) Pham, W.; Cassell, L.; Gillman, A.; Koktysh, D.; Gore, J. C. A near-Infrared Dye for Multichannel Imaging. *Chem. Commun.* **2008**, 1895−1897.
(15) Antaris, A. L.; Chen, H.; Diao, S.; Ma, Z.; Zhang, Z.; Zhu, S.; Wang, J.; Lozano, A. X.; Fan, Q.; Chew, L.; Zhu, M.; Cheng, K.; Hong, X.; Dai, H.; Cheng, Z. A High Quantum Yield Molecule-Protein Complex Fluorophore for Near-Infrared II Imaging. *Nat. Commun.* **2017**, *8*, 15269.
(16) Siebrand, W. Radiationless Transitions in Polyatomic Molecules. I. Calculation of Franck—Condon Factors. *J. Chem. Phys.* **1967**, *46*, 440−447.
(17) Siebrand, W. Radiationless Transitions in Polyatomic Molecules. Ii. Triplet-Ground-State Transitions in Aromatic Hydrocarbons. *J. Chem. Phys.* **1967**, *47*, 2411−2422.
(18) Caspar, J. V.; Sullivan, B. P.; Kober, E. M.; Meyer, T. J. Application of the Energy Gap Law to the Decay of Charge Transfer Excited-States. Solvent Effects. *Chem. Phys. Lett.* **1982**, *91*, 91−95.
(19) Englman, R.; Jortner, J. The Energy Gap Law for Radiationless Transitions in Large Molecules. *Mol. Phys.* **1970**, *18*, 145−164.
(20) McNamara, L. E.; Liyanage, N.; Peddapuram, A.; Murphy, J. S.; Delcamp, J. H.; Hammer, N. I. Donor-Acceptor-Donor Thienopyrazines Via Pd-Catalyzed C-H Activation as Nir Fluorescent Materials. *J. Org. Chem.* **2016**, *81*, 32−42.
(21) Alander, J. T.; Kaartinen, I.; Laakso, A.; Patila, T.; Spillmann, T.; Tuchin, V. V.; Venermo, M.; Välisuo, P. A Review of Indocyanine Green Fluorescent Imaging in Surgery. *Int. J. Biomed. Imaging* **2012**, *2012*, 940585.
(22) Alander, J. T.; Villet, O. M.; Pätilä, T.; Kaartinen, I. S.; Lehecka, M.; Nakaguchi, T.; Suzuki, T.; Tuchin, V. *Fluorescence Imaging for Surgeons: Review of Indocyanine Green Imaging in Surgery*; Springer: Cham, 2015.
(23) Huckaba, A. J.; Giordano, F.; McNamara, L. E.; Dreux, K. M.; Hammer, N. I.; Tschumper, G. S.; Zakeeruddin, S. M.; Grätzel, M.; Nazeeruddin, M. K.; Delcamp, J. H. Indolizine-Based Donors as Organic Sensitizer Components for Dye-Sensitized Solar Cells. *Adv. Energy Mater.* **2015**, *5*, 1401629.
(24) Zhang, Y.; Autry, S. A.; McNamara, L. E.; Nguyen, S. T.; Le, N.; Brogdon, P.; Watkins, D. L.; Hammer, N. I.; Delcamp, J. H. Near-Infrared Fluorescent Thienothiadiazole Dyes with Large Stokes Shifts and High Photostability. *J. Org. Chem.* **2017**, *82*, 5597−5606.
(25) McNamara, L. E.; Rill, T. A.; Huckaba, A. J.; Ganeshraj, V.; Gayton, J.; Nelson, R. A.; Sharpe, E. A.; Dass, A.; Hammer, N. I.; Delcamp, J. H. Indolizine-Squaraines: NIR Fluorescent Materials with Molecularly Engineered Stokes Shifts. *Chem. - Eur. J.* **2017**, *23*, 12494−12501.
(26) Huckaba, A. J.; Yella, A.; McNamara, L. E.; Steen, A. E.; Murphy, J. S.; Carpenter, C. A.; Puneky, G. D.; Hammer, N. I.; Nazeeruddin, M. K.; Grätzel, M.; Delcamp, J. H. Molecular Design Principles for Near-Infrared Absorbing and Emitting Indolizine Dyes. *Chem. - Eur. J.* **2016**, *22*, 15536−15542.
(27) Mustroph, H.; Towns, A. Fine Structure in Electronic Spectra of Cyanine Dyes: Are Sub-Bands Largely Determined by a Dominant Vibration or a Collection of Singly Excited Vibrations? *ChemPhysChem* **2018**, *19*, 1016−1023.
(28) Qian, G.; Dai, B.; Luo, M.; Yu, D.; Zhan, J.; Zhang, Z.; Ma, D.; Wang, Z. Y. Band Gap Tunable, Donor-Acceptor-Donor Charge-Transfer Heteroquinoid-Based Chromophores: Near Infrared Photoluminescence and Electroluminescence. *Chem. Mater.* **2008**, *20*, 6208−6215.
(29) Bai, M.; Achilefu, S. Synthesis and Spectroscopy of near Infrared Fluorescent Dyes for Investigating Dichromic Fluorescence. *Bioorg. Med. Chem. Lett.* **2011**, *21*, 280−284.
(30) Dost, T. L.; Gressel, M. T.; Henary, M. Synthesis and Optical Properties of Pentamethine Cyanine Dyes with Carboxylic Acid Moieties. *Anal. Chem. Insights* **2017**, *12*, 117739011771193.
(31) Frisch, M. J.; Trucks, G. W.; Schlegel, H. B.; Scuseria, G. E.; Robb, M. A.; Cheeseman, J. R.; Scalmani, G.; Barone, V.; Petersson, G. A.; Nakatsuji, H.; Li, X.; Caricato, M.; Marenich, A. V.; Bloino, J.; Janesko, B. G.; Gomperts, R.; Mennucci, B.; Hratchian, H. P.; Ortiz, J. V.; Izmaylov, A. F.; Sonnenberg, J. L.; Williams-Young, D.; Ding, F.; Lipparini, F.; Egidi, F.; Goings, J.; Peng, B.; Petrone, A.; Henderson, T.; Ranasinghe, D.; Zakrzewski, V. G.; Gao, J.; Rega, N.; Zheng, G.; Liang, W.; Hada, M.; Ehara, M.; Toyota, K.; Fukuda, R.; Hasegawa, J.; Ishida, M.; Nakajima, T.; Honda, Y.; Kitao, O.; Nakai, H.; Vreven, T.; Throssell, K.; Montgomery, J. A., Jr.; Peralta, J. E.; Ogliaro, F.;

DOI: 10.1021/acs.joc.8b02521
J. Org. Chem. 2019, 84, 687−697

Bearpark, M. J.; Heyd, J. J.; Brothers, E. N.; Kudin, K. N.; Staroverov, V. N.; Keith, T. A.; Kobayashi, R.; Normand, J.; Raghavachari, K.; Rendell, A. P.; Burant, J. C.; Iyengar, S. S.; Tomasi, J.; Cossi, M.; Millam, J. M.; Klene, M.; Adamo, C.; Cammi, R.; Ochterski, J. W.; Martin, R. L.; Morokuma, K.; Farkas, O.; Foresman, J. B.; Fox, D. J. *Gaussian 16*, revision A.03; Gaussian, Inc.: Wallingford, CT, 2016.

(32) Zhao, Y.; Truhlar, D. G. The M06 Suite of Density Functionals for Main Group Thermochemistry, Thermochemical Kinetics, Noncovalent Interactions, Excited States, and Transition Elements: Two New Functionals and Systematic Testing of Four M06-Class Functionals and 12 Other Functionals. *Theor. Chem. Acc.* **2008**, *120*, 215−241.

(33) Marenich, A. V.; Cramer, C. J.; Truhlar, D. G. Universal Solvation Model Based on Solute Electron Density and on a Continuum Model ofthe Solvent Defined by the Bulk Dielectric Constant and Atomic Surface Tensions. *J. Phys. Chem. B* **2009**, *113*, 6378−6396.

(34) Cao, J.; Fan, J.; Sun, W.; Guo, Y.; Wu, H.; Peng, X. The Photoprocess Effects of an Amino Group Located at Different Positions Along the Polymethine Chain in Indodicarbocyanine Dyes. *RSC Adv.* **2017**, *7*, 30740−30746.

(35) Williams, A. T. R.; Winfield, S. A.; Miller, J. N. Relative Fluorescence Quantum Yields Using a Computer-Controlled Luminescence Spectrometer. *Analyst* **1983**, *108*, 1067−1071.

(36) Reindl, S.; Penzkofer, A.; Gong, S.-H.; Landthaler, M.; Szeimies, R. M.; Abels, C.; Bäumler, W. Quantum yield of triplet formation for indocyanine green. *J. Photochem. Photobiol., A* **1997**, *105*, 65−68.

(37) *APEX3; Programs for X-Ray Data Collection and Reduction*; Bruker-AXS Inc.: Madison, WI, USA, 2016.

(38) Krause, L.; Herbst-Irmer, R.; Sheldrick, G. M.; Stalke, D. Comparison of Silver and Molybdenum Microfocus X-Ray Sources for Single-Crystal Structure Determination. *J. Appl. Crystallogr.* **2015**, *48*, 3−10.

(39) Sheldrick, G. M. Crystal Structure Refinement with SHELXL. *Acta Crystallogr., Sect. C: Struct. Chem.* **2015**, *71*, 3−8.

(40) Sheldrick, G. M. SHELXT - Integrated Space-Group and Crystal-Structure Determination. *Acta Crystallogr., Sect. A: Found. Adv.* **2015**, *71*, 3−8.

(41) Spek, A. L. Platon Squeeze: A Tool for the Calculation of the Disordered Solvent Contribution to the Calculated Structure Factors. *Acta Crystallogr., Sect. C: Struct. Chem.* **2015**, *71*, 9−18.

DOI: 10.1021/acs.joc.8b02521
J. Org. Chem. 2019, 84, 687−697